

# Differential Fluorescence Quenching of Fluorescent Nucleic Acid Base Analogues by Native Nucleic Acid Monophosphates

Madhavan Narayanan,<sup>†</sup> Goutham Kodali,<sup>†</sup> Yangjun Xing,<sup>†</sup> Mary E. Hawkins,<sup>‡</sup> and Robert J. Stanley<sup>\*,†</sup>

Department of Chemistry, Temple University, Philadelphia, Pennsylvania 19122, and Laboratory of Receptor Biology and Gene Expression, Pediatric Oncology Branch, Bethesda, Maryland 20854

Received: February 5, 2010; Revised Manuscript Received: March 15, 2010

Fluorescent nucleic acid base analogues (FBAs) are used widely as probes of DNA and RNA structure and dynamics. Of increasing utility are the pteridone adenosine analogues (6MAP, DMAP) and pteridine guanosine analogues (3MI, 6MI). These FBAs (collectively referred to as PTERs) are useful, in part, because their fluorescence quantum yields,  $\Phi_f$ , are modulated by base stacking with native bases (NBs), making them sensitive reporters of DNA structure. The quenching mechanism has been hypothesized to be photoinduced electron transfer following selective excitation of the FBA, but hard evidence for this has been lacking. The degree of quenching shows some dependence on the neighboring bases, but there has been no real determination as to whether FBA\*:NB complexes satisfy the basic thermodynamic requirement for spontaneous PET: a negative free energy for the electron transfer reaction. Indeed, quenching may result from entirely different mechanisms. To address these questions, Stern–Volmer (S–V) experiments were performed using the native-base monophosphate nucleotides (NMPs) GMP, AMP, CMP, and dTMP in aqueous solutions as quenchers to obtain quenching rate constants,  $k_q$ . Cyclic voltammetry (CV) and optical absorption and emission data of the PTERs were obtained in aprotic organic solvents. These data were used to obtain excited-state redox potentials from which electron transfer free energies were derived using the Rehm–Weller equation. The reorganization energies for PET were obtained using the Scandola–Balzani equation, taking into account the free energy contribution due to water. 6MAP\*, DMAP\*, and 3MI\* gave negative free energies between  $-0.1$  and  $-0.2$  eV and reorganization energies of about 0.13 eV. They all displayed ET activation energies below the accessible thermal energy ( $0.038$  eV =  $3/2k_B T$ , where  $k_B$  is Boltzmann's constant) for all NMPs with the exception of CMP, whose activation barrier was only about 35% higher ( $\sim 0.05$  eV). Thus, we conclude that these PTERs act as electron acceptors and promote NMP oxidation. However, 6MI\* had positive ET free energies for all NMPs with the exception of GMP (and then only for nucleobase oxidation). The magnitudes of these free energies ( $\geq 0.45$  eV for AMP, CMP, and dTMP) suggest that 6MI\* may not be quenched by PET.

## Introduction

Understanding the structure and function of nucleic acids is a prerequisite toward understanding basic biological processes such as replication, transcription, and DNA repair. Fluorescence spectroscopy is particularly valuable and widely used as a probe of local structure and function because it is noninvasive. As the native bases (NBs) are nonfluorescent, fluorophores have been developed that can be added as selective tags to oligonucleotides. A large set of fluorophores are now commercially available that can be attached almost anywhere along the DNA backbone (fluorescein is a common example). Intercalation into the major or minor groove (e.g., ethidium bromide) is another common approach to render DNA/RNA fluorescent. Because they do not participate in Watson–Crick (WC) base pairing, and sometimes distort helical structure, these types of fluorescent probes are not suitable for reporting on local changes in the helical structure and dynamics of DNA and RNA.

In order to overcome this disadvantage, structural analogues of native nucleic acids have been explored which are fluorescent

but form WC base pairs.<sup>1,2</sup> In the best cases, these fluorescent base analogues (FBAs) alter the native structure of helical DNA minimally, while allowing for selective optical excitation and detection. In many FBAs, the fluorescence quantum yield can be very sensitive to changes in base stacking,<sup>3–11</sup> making them uniquely suited to studying helical structure and dynamics. However, the quenching mechanism often depends on sequence, particularly the identity of the neighboring bases stacked 5' and 3' to the FBA.

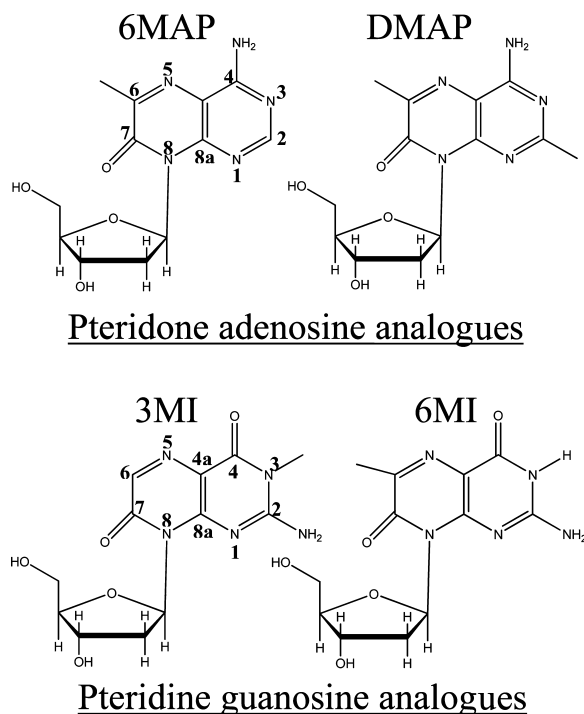
The most widely exploited FBA is 2-aminopurine (2AP),<sup>12</sup> the 2-amino analogue of adenine (6-aminopurine). Studies on the quenching of 2AP\* suggest that photoinduced electron transfer is operative as the quenching pathway. Most of the evidence for this conclusion comes from time-resolved spectroscopy, although not all groups agree on this interpretation of the data.<sup>13–16</sup> We have recently obtained 2AP oxidation and reduction potentials by cyclic voltammetry<sup>17</sup> in aprotic organic solvents. These results were coupled with fluorescence quenching (Stern–Volmer) experiments to support the hypothesis of PET in 2AP:native-base monophosphate nucleotide (NMP) complexes.

Other FBAs have been synthesized, allowing substitutions for adenine (e.g., 6MAP,<sup>18</sup> 8-vinyladenine<sup>19</sup>), guanine (3MI and

\* To whom correspondence should be addressed. E-mail: rstanley@temple.edu.

<sup>†</sup> Temple University.

<sup>‡</sup> Laboratory of Receptor Biology and Gene Expression.

**SCHEME 1: Chemical Structures of the FBAs Used in This Study**


6MI),<sup>20</sup> and cytosine (pyrrolo-C and pyrrolo-dC).<sup>21</sup> There are fewer FBAs for thymine and uracil (5-methyl-2-pyrimidinone)<sup>22,23</sup> that have high fluorescence yields while still mimicking the double helical structure of native DNA or RNA. The mechanism of fluorescence quenching has remained largely undiscovered.

We have used the cytidine analogue pyrrolo-dC,<sup>10</sup> the adenine analogue 6MAP,<sup>8</sup> as well as 2AP<sup>3,9</sup> to explore the role of base flipping in the cyclobutylpyrimidine dimer repair protein DNA photolyase. In each case, we could not rationalize the degree of fluorescence quenching based solely on the identity of the bases neighboring the FBA.

6MAP belongs to the pteridine/pteridone (abbreviated PTER) class of analogues (see Scheme 1) developed and characterized by Pfeleiderer and Hawkins.<sup>7,18,20,24</sup> These include the adenosine analogue 6MAP and its dimethyl form DMAP and the guanosine analogues 3MI and 6MI. The molecules are highly fluorescent as monomers but quench to varying degrees upon base stacking.<sup>25</sup> The PTER backbone affords a significantly red-shifted absorption of the lowest energy bright transition compared to the NBs. These FBAs have maximal absorption around 340 nm with extinction coefficients ranging from 8500 to 14 000 M<sup>-1</sup> cm<sup>-1</sup>, a large value for WC FBAs. Equally impressive is that the emission is red-shifted by 100 nm to about 430 nm. This combination of selective excitation and an emission wavelength that coincides with the peak quantum efficiency of many photomultipliers make a strong case for the wider utilization of PTERs.

This study was undertaken to answer the following questions about this new class of probes: (1) Is there an inherent preference for certain native nucleic acids (e.g., purines vs pyrimidines) to quench the fluorescence of these FBAs? (2) Is the quenching mechanism photoinduced electron transfer? (3) If the FBAs are quenched by PET, is the photoexcited FBA (FBA\*) the donor or acceptor? The answer to these questions must involve a determination of the excited-state oxidation and reduction potentials of the PTERs and whether these redox potentials are sufficient to promote spontaneous electron transfer when com-

plexed with the NBs. We now describe our approach to this determination.

Stern–Volmer (S–V) quenching experiments<sup>26</sup> have been used to obtain the quenching rate between an excited-state donor (or acceptor) and its quencher. While the S–V approach does not identify the quenching mechanism, it provides the quenching rate constant that must be determined to push the question of PET further.

If the radiative lifetime of the fluorophore,  $\tau_0$ , is known, then the ratio of unquenched to quenched integrated fluorescence,  $I_0/I$ , can be measured as a function of quencher concentration  $[Q]$  to obtain the quenching rate constant,  $k_q$ :

$$\left(\frac{I_0}{I}\right) = 1 + k_q\tau_0[Q] \quad (1a)$$

$$\left(\frac{I_0}{I}\right) = B + (K_S + K_d)[Q] + K_S K_d [Q]^2 \quad (1b)$$

A modified form of the S–V equation that takes into account static quenching (eq 1b) can be used if there is evidence of complex formation. In this case, the equilibrium constant for the formation of ground-state complexes (which are quenched),  $K_S$ , and the constant for dynamic quenching,  $K_d$ , are separated (the intercept,  $B$ , is typically unity but can be varied as described below to obtain a better fit). If  $\tau_0$  is known, then  $k_q = K_d/\tau_0$ .

If quenching is due to electron transfer, then these  $k_q$  are related to  $k_{ET}$ , the rate constant for (photoinduced) electron transfer.<sup>27</sup> There are various approaches to finding the relationship between  $k_q$  and the driving force and reorganization energies,  $\Delta G_{ET}^\circ$  and  $\lambda_0$ , respectively, for the PET reaction, starting with the semiclassical Marcus relation.<sup>28</sup> However, when the diffusion rate of the reactants is slower than ET, other approaches have been employed. The Rehm–Weller equation<sup>29</sup> is widely used, but the activation energy was derived in this treatment empirically. We have chosen the treatment of Scandola–Balzani<sup>29</sup> which is based on the bond energy–bond order method.<sup>30</sup> Both treatments recognize that the upper limit for collisional quenching must be the diffusion rate. Either approach requires knowledge of the excited-state reduction and oxidation potentials of the FBAs. The excited-state reduction and oxidation potentials, which are not known *a priori*, were calculated using the  $S_0 \rightarrow S_1$  transition energy,  $E_{00}$ , and the ground-state reduction and oxidation potentials,<sup>31</sup> which we have measured by cyclic voltammetry (*vide infra*).

The free energies for electron transfer,  $\Delta G_{ET}^\circ$ , and the activation energy,  $E_{ET}^\ddagger$ , retrieved from this procedure have enabled us to assign the direction of electron transfer, assuming that it is responsible for fluorescence quenching in these FBAs. We show that the activation energies derived in this manner correlate well with the magnitudes of the experimental  $k_q$  for 6MAP\*, DMAP\*, and 3MI\* and suggest the FBAs are quenched by nucleobase oxidation. 6MI\* appears to quench *via* electron transfer by both nucleobase oxidation *and* reduction.

**Materials and Methods**

Guanosine monophosphate (GMP), adenosine monophosphate (AMP), cytidine monophosphate (CMP), and deoxythymidine monophosphate (dTMP) were purchased from Sigma Aldrich and used as received for fluorescence quenching experiments. 18 M $\Omega$  cm<sup>-1</sup> distilled/deionized water was used to make all aqueous solutions. The PTER FBAs were obtained as described in refs 18 and 25. They were purified using reverse phase HPLC

on a YMC-AQ C-18 column using an acetonitrile (ACN)/water gradient (10–15% ACN over 20 min). HPLC grade ACN from ACROS and HPLC grade water from Fisher Scientific were used for this purpose. Formic acid was added to both ACN and water to a final concentration of 0.1%.

The concentrations of the samples for fluorescence experiments were determined in 0.1 M potassium phosphate buffer pH 7.0 by UV/vis absorption spectroscopy using a HP8452A diode array spectrophotometer. The following extinction coefficients were used: GMP ( $\epsilon_{260} = 12\,080\text{ M}^{-1}\text{ cm}^{-1}$ ),<sup>32</sup> AMP ( $\epsilon_{260} = 15\,020\text{ M}^{-1}\text{ cm}^{-1}$ ),<sup>32</sup> CMP ( $\epsilon_{260} = 7070\text{ M}^{-1}\text{ cm}^{-1}$ ),<sup>32</sup> dTMP ( $\epsilon_{260} = 8560\text{ M}^{-1}\text{ cm}^{-1}$ ),<sup>32</sup> 6MAP ( $\epsilon_{329} = 8500\text{ M}^{-1}\text{ cm}^{-1}$ ),<sup>18</sup> DMAP ( $\epsilon_{334} = 8912\text{ M}^{-1}\text{ cm}^{-1}$ ),<sup>18</sup> 3MI ( $\epsilon_{351} = 13\,000\text{ M}^{-1}\text{ cm}^{-1}$ ),<sup>33</sup> and 6MI ( $\epsilon_{341} = 14\,125\text{ M}^{-1}\text{ cm}^{-1}$ ).<sup>34</sup>

The steady-state fluorescence of the various FBA:NMP pairs was measured as described in detail previously.<sup>17</sup> Briefly, the concentration of the FBAs was fixed at  $1\ \mu\text{M}$  and the NMP concentrations were varied from 0.01 to 50.0 mM. The excitation and emission slits were 2 and 5 nm, respectively, for the pteridones and 2 and 3 nm, respectively, for the pteridines. Both excitation and emission light was unpolarized. The wavelength range of the integration depended on the specific FBA but encompassed a minimum of 300 nm. Origin (v. 7.0, OriginLab Inc.) was used to obtain fits of eq 1b to these data. The  $R^2$  values obtained from the fit were at least 0.99. Matlab R14 (The Mathworks) was used to construct sensitivity plots from a wide range of initial parameter sets so that the obtained fit for  $\Delta G_{\text{W}}^{\circ}$  and  $\lambda_0$  did not end up in local minima.

Time-resolved fluorescence decays were collected on a PTI Q25 Quantmaster using a 340 nm LED source. The repetition rate was 1 kHz. The time base was stepped logarithmically over a span of  $\sim 160$  ns in 200 channels. The emission slit was centered at 430 nm with a band-pass of 25 nm. The instrument response function (IRF) was collected using the same cuvette by replacing the sample solution with a silica colloid. The decay data were fitted using the raw IRF based on a convolute-and-compare algorithm implemented in the instrument software.

CV measurements were performed at 20 °C on 1.0 mM solutions of FBAs using a CH610C electrochemical analyzer (CH Instruments, Inc., Texas) as described in detail previously.<sup>17</sup>

Theoretical one-electron redox potentials of the FBAs were calculated using density functional theory (DFT) on the methylated form using Gaussian 03 (v.c02).<sup>35</sup> The 8-methyl form of the pteridines/pteridones was used instead of the nucleosides in order to reduce computational time. A polarizable continuum model (PCM) was used to calculate redox potentials of FBAs in ACN and DMF. More details about these calculated potentials, including estimates of the neutral, radical cation, and anion energies in a PCM “solvent” can be found in Table S.2 of the Supporting Information. The structures of the FBAs were first optimized *in vacuo* at the Hartree–Fock level of theory followed by DFT using a B3LYP/6-31+G(d,p) functional/basis set. These optimized structures were used as the initial geometry for PCM calculations in ACN ( $\epsilon = 35.9$ ) and DMF ( $\epsilon = 36.7$ )<sup>36</sup> using the PCM.<sup>37–39</sup> These structures were analyzed carefully to make sure none had imaginary frequencies. The relative energies of FBA tautomers in a vacuum were calculated using SPARTAN molecular modeling software (version 4 essential edition).

## Results

**Fluorescence Quenching of FBAs: Buffer Quenching.** The steady-state fluorescence of the various FBA:NMP pairs was measured as a function of NMP concentration (see Figure 1).

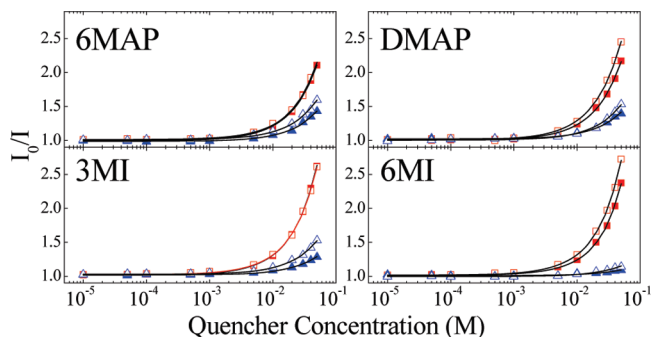


**Figure 1.** S–V plots for the various FBAs quenched by GMP (□), AMP (■), CMP (▲), and dTMP (△). All fluorescence quenching measurements were made in potassium phosphate buffer, pH 7.0 at 20 °C. The solid black lines are fits to the data using the modified Stern–Volmer equation (see eq 1b). The fit parameters are tabulated in Table 1.

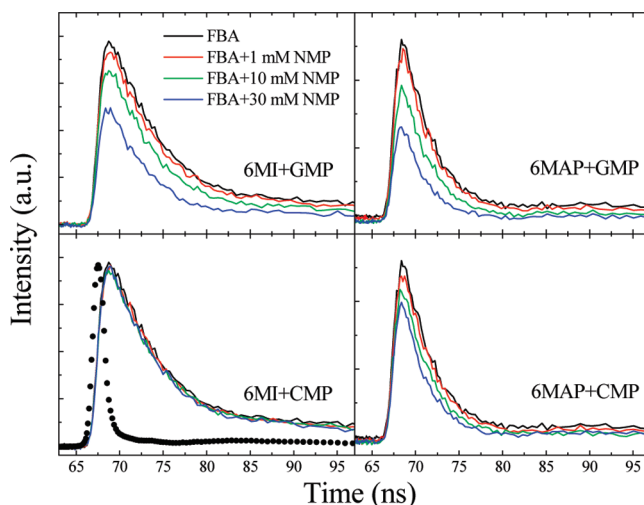


**Figure 2.** Time-resolved emission of 6MI and 6MAP with various concentrations of quenchers GMP and CMP. 310 nm excitation was used, and emission was detected at 430 nm. The instrument response function is shown (●) in the 6MI+CMP panel.

To interpret these data, it was necessary to ascertain whether buffer quenching or complexation was active. Ions have been known to quench dye fluorescence.<sup>40,41</sup> We measured the emission of 3MI over a concentration range of 0.0–0.1 M phosphate and observed no significant quenching due to buffer at pH 7.0. Data was also taken for 3MI:GMP in water only. 3MI was chosen because its emission is insensitive to pH.<sup>24,42</sup> The  $K_d$  value was about 30% higher than the buffered solution, suggesting that  $k_d$  is higher in the absence of buffer (results not shown). Interestingly,  $K_S$  was about 40% lower than the buffered case, suggesting that solvation by ions shielded the molecules from reactive collisions.

**Time-Resolved Emission Studies of FBA:NMP Complexes.** Representative decays were taken on pteridine/pteridone bases with purine/pyrimidine quenchers. Data was collected on 6MI and 6MAP monomers and complexes with GMP and CMP over a range of concentrations to determine whether complexation led to noncollisional excited-state quenching. Static quenching appears as a decrease in emission intensity with no change in lifetime, while dynamic quenching shows a concentration-dependent decrease in  $\tau_0$ . Of course, both quenching mechanisms can occur simultaneously.

The data are shown in Figure 2. The FBAs at  $[\text{NMP}] = 0$  each gave two lifetimes. The fast component, ca. 5 ns, had more than 99% of the amplitude, which we assigned as the radiative

**TABLE 1: Fluorescence Quenching Constant,  $k_q = K_d/\tau_0$ , of the FBAs against Various Nucleotide Quenchers as Derived from Fitting the  $I_0/I$  vs  $[Q]$  Data Using the Modified Stern–Volmer Equation (eq 1b)<sup>a</sup>**

FBA	$\tau_0$ (ns)	NB	$B$ ( $\pm 0.01$ )	$K_d$ ( $M^{-1}$ )	$K_S$ ( $M^{-1}$ )	$k_q(\times 10^{-9})$ ( $M^{-1} s^{-1}$ )
6MAP	3.8 <sup>18</sup>	G	1.01	19.88 (2.60)	1.45 (1.59)	5.20
		A	1.00	20.88 (1.09)	0.70 (0.58)	5.46
		C	0.99	8.06 (2.88)	0.62 (2.18)	2.11
		dT	1.01	11.68 (0.34)	0.00 (0.01)	3.05
DMAP	4.8 <sup>18</sup>	G	1.00	22.51 (1.24)	0.28 (0.62)	4.67
		A	1.01	28.04 (1.93)	0.43 (0.87)	5.81
		C	1.02	7.87 (0.21)	0 (NA)	1.63
		dT	1.00	10.42 (0.24)	0 (NA)	2.16
3MI	6.5 <sup>20</sup>	G	1.02	26.25 (1.54)	2.63 (0.79)	4.03
		A	1.02	26.27 (1.76)	2.36 (0.89)	4.03
		C	1.02	5.43 (0.14)	0.00 (NA)	0.83
		dT	1.03	9.36 (2.67)	0.37 (1.91)	1.44
6MI	6.4 <sup>24 b</sup>	G	1.01	12.10 (8.46)	9.24 (7.75)	1.89
		A	1.02	25.96 (2.07)	3.41 (1.10)	4.06
		C	1.01	1.70 (0.15)	0 (NA)	0.27
		dT	1.00	3.10 (0.12)	0 (NA)	0.48

<sup>a</sup> The fitting error in  $k_q$  is given in parentheses.  $K_S$  represents the equilibrium constant for ground-state complexation, and  $B$  is the fitted  $y$ -intercept. <sup>b</sup> The lifetime used here is a weighted lifetime from a biexponential fit with  $\tau_1 = 5.45$  ns ( $\alpha_1 = 0.20$ ) and  $\tau_2 = 6.58$  ns ( $\alpha_2 = 0.80$ ).

lifetime of the FBA (see Table S.1 of the Supporting Information). The second component was several orders of magnitude slower and was identified as a baseline component. The ratios of the prompt lifetimes,  $\tau_0/\tau$ , where  $\tau_0$  is the lifetime at  $[NMP] = 0$ , were plotted, and the slopes were obtained by a linear fit for comparison with S–V analyses based on steady-state emission intensity data (see Figure S.1 of the Supporting Information).

The time-resolved emission of FBAs with GMP or CMP was taken from 1 to 50 mM in 0.1 M phosphate buffer at pH 7 and 20 °C. Interestingly, 6MI:CMP complexes showed only small changes in amplitude and lifetime ( $\tau_0/\tau$  slope  $\sim 1.2$ ). Similar behavior was observed for aromatic pterins quenched by dNMPs.<sup>43</sup> CMP quenched 6MAP with an intermediate slope of about 6. The slopes for 6MI and 6MAP with GMP were approximately 9. These results suggest that both static and dynamic quenching contribute to the observed fluorescence decay. This fact requires a modified treatment of the steady-state emission data as described next.

**Modified Stern–Volmer Analysis of Steady-State Emission Quenching.** The integrated steady-state fluorescence intensities for the various FBA:NMP pairs were fitted to the modified Stern–Volmer equation (eq 1b) to obtain  $K_S$ ,  $K_d$ , and  $B$ , as summarized in Table 1. The intercept,  $B$ , was included because of evidence of instrumental error at very low concentrations of quencher. This intercept was only a few percent from 1.00 for all cases.  $k_q$  can be obtained from  $K_d$  as described above if  $\tau_0$  is known. The  $\tau_0$  values<sup>16,18,20,44,45</sup> used for the analyses are all monoexponential lifetimes except in the case of 6MI, which showed a biexponential emission decay. Here, a weighted lifetime was used (see Table 1).

6MAP and DMAP are pteridone adenosine analogues. Both showed a preference for quenching by purines. 6MAP is quenched by AMP and GMP about equally, whereas  $k_q$  for dTMP is about a factor of 2 lower, with CMP quenching about 30% lower still, AMP  $\sim$  GMP  $>$  dTMP  $>$  CMP. DMAP, a dimethylated form of 6MAP, exhibited similar quenching behavior as 6MAP with purines being more efficient than

pyrimidines, AMP  $>$  GMP  $>$  dTMP  $>$  CMP. DMAP is preferentially quenched by AMP; its  $k_q$  is about 20% higher than GMP. dTMP is again somewhat more efficient than CMP, but both pyrimidines appear to be less efficient quenchers for DMAP than for 6MAP. 6MAP and DMAP appear to form ground-state complexes with DMAP being the weaker in this regard. This was also observed in the time domain for 6MAP with GMP and CMP as described above (Table 1,  $K_S$ , and Figure 2). However, the pyrimidines seem to have significantly less propensity for complexation than purines.

3MI and 6MI are pteridine analogues of guanosine. 3MI is quenched about equally by GMP or AMP and significantly less efficiently by the pyrimidines but shows the same overall ordering as 6MAP: GMP  $\sim$  AMP  $\gg$  dTMP  $>$  CMP. Overall, the  $k_q$  values are lower than the corresponding values for the pteridones. This is true especially for the pyrimidines. Indeed, the quenching constants for 3MI by pyrimidines are about a factor of 3 lower than that for 6MAP or DMAP (or 2AP for that matter<sup>17</sup>). This observation is discussed further below. 3MI shows a tendency to form complexes with purines but not pyrimidines.

6MI shows a substantial preference for quenching by purines but is quenched most effectively by AMP instead of GMP: AMP  $>$  GMP  $>$  dTMP  $\sim$  CMP. 6MI quenching by pyrimidines is an order of magnitude lower than purine quenching and is significantly lower than that experienced by the other FBAs. The  $K_S$  values for 6MI:purines are rather high, as was corroborated by the time-resolved emission studies. The fitted value of  $K_S = 0$  for both C and dT was also observed in these studies.

The enhanced quenching of purines appears to marginalize the significance of Watson–Crick (WC) base pairing in complex formation. If base pairs were stabilized through WC hydrogen bonding, then we would expect to see this effect in the  $k_q$  constants for 6MAP, and DMAP with T, and 3MI and 6MI with C. No straightforward correlation appears, perhaps because complexes formed via WC base pairing might not undergo quenching because there is no overlap of the relevant orbitals for electron transfer. Given that the solvent is water, there is no significant energetic advantage for WC complexes to form.

**Cyclic Voltammetry (CV) of FBAs.** CV measurements were performed on FBAs in two electrolyte systems as described above. Since only ACN could provide a high enough positive potential,  $E_{OX}^\circ$  values were obtained in that solvent.  $E_{RED}^\circ$  values measured in DMF were used in subsequent calculations, as the cathodic part of the CV scan is better resolved in DMF but appears truncated and diminished in ACN solvent. As a test, the measured CV of thymidine in ACN (data not shown) was in excellent agreement with that reported by Seidel et al.<sup>31</sup> All experimental redox values have an uncertainty of  $\pm 0.05$  V.

CV scans of the FBAs are shown in Figure 3. The FBAs all exhibited irreversible electrochemistry. This has been observed for the native nucleic acids<sup>31</sup> as well. The pteridones/pteridines had multiple reduction features (see Figure 3, dimethylformamide column), while the oxidation range gave one major peak (see Figure 3, first column). The first reduction peak seen for the pteridones/pteridines was assigned as FBA + e<sup>-</sup>  $\rightarrow$  FBA<sup>-</sup>. Peaks at greater negative potential are presumably due to the reduction of species generated in follow-up reactions of FBA<sup>-</sup>, the chemical identity of which is unknown (Figure 2, second column). The single major peak obtained for oxidation was assigned as FBA  $\rightarrow$  FBA<sup>+</sup> + e<sup>-</sup>.

CV measurements were performed as a function of concentration (1–3 mM) to ascertain whether dimerization affected the shape of the CV curve. The current was proportional to the

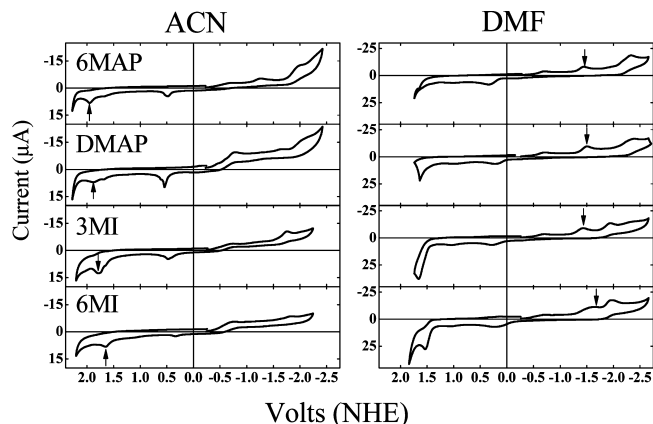


**Figure 3.** CVs of FBAs in ACN/0.1 M TBAF (left) and in DMF/0.1 M TBAF (right). A 100 mV/s scan rate was used for these scans. All scans were initiated in the negative scan direction. The arrows indicate the oxidation and reduction peaks used in the calculation of the excited-state redox potentials.

**TABLE 2: Comparison of FBA Experimental ( $E_{\text{redox}}^{\circ\text{EXP}}$ ) and Calculated ( $E_{\text{redox}}^{\circ\text{C}}$ ) Redox Potentials<sup>a</sup>**

	ACN		DMF		ACN		DMF	
	$E_{\text{OX}}^{\circ\text{EXP}}$	$E_{\text{OX}}^{\circ\text{C}}$	$E_{\text{OX}}^{\circ\text{EXP}}$	$E_{\text{OX}}^{\circ\text{C}}$	$E_{\text{RED}}^{\circ\text{EXP}}$	$E_{\text{RED}}^{\circ\text{C}}$	$E_{\text{RED}}^{\circ\text{EXP}}$	$E_{\text{RED}}^{\circ\text{C}}$
6MAP	<b>1.95</b>	1.84	NM	1.84	-1.97	-1.63	<b>-1.46</b>	-2.37
DMAP	<b>1.88</b>	1.75	NM	1.75	-2.04	-1.72	<b>-1.50</b>	-2.42
3MI	<b>1.79</b>	1.69	1.68	1.69	-1.76	-1.76	<b>-1.44</b>	-1.96
6MI	<b>1.65</b>	1.49	1.54	1.50	-1.85	-1.89	<b>-1.68</b>	-1.96

<sup>a</sup> The experimental potentials used are highlighted in bold and indicate the majority species, and they are used for further analysis. All of the potentials reported here are referenced to the NHE. NM = not measurable.

concentration. Absorption spectra taken as a function of concentration showed no spectral shifts or line shape changes, providing additional assurance that the doublet structure in the voltammograms was not due to dimers. Scan rates were varied from 50 mV/s to 1 V/s without producing a significant alteration of the shape of the voltammogram.

We calculated the ground-state energies of the different tautomers and found that the keto/amine species were more stable than the corresponding enol/imine form. For example, 6MI has the smallest energy gap between the keto/amine and enol/imine forms, about -12 kJ/mol. At room temperature, the keto/amine form would be present at greater than 99%. On the basis of this analysis, we rule out tautomers as the origin of the minor CV peaks. Although FBA solutions were kept anhydrous, it is possible that trace amounts of water produced small amounts of differently protonated FBAs. On the basis of these considerations, the least negative peak was assigned as the reduction potential (see arrows in Figure 3, second column).

Calculated redox potentials of the FBAs were obtained from the free energy changes for the formation of the radical cation or anion and subtracting from this the energy of the neutral FBA, according to the method of Datta et al.<sup>46</sup> (see Table 2, columns 3, 5, 7, and 9). We have made the assumption that the sugar moiety does not affect the redox potential of the FBA significantly. The effect of different basis sets on the calculated redox potentials for 9-methyl-2AP was tested.<sup>17</sup> No significant improvement in the redox potentials was observed beyond the 6-31+G(d,p) level, even though the energies of the neutral, cation, or anion states varied as much as 100 kcal/mol ( $\Delta E_{\text{PCM}}$ , see eq 2) between the most widely differing diffuse basis sets. This agreement can be ascribed to cancellation of errors when

taking the energy difference of the neutral and radical. On the basis of this analysis, the 6-31+G(d,p) basis set was used for the pteridine/pteridone calculations.

The free energy of each molecule,  $G^\circ$ , was then calculated as described in ref 17

$$G^\circ = E_{\text{PCM}} + E_{\text{Thermal}} - TS \quad (2)$$

The redox free energies,  $\Delta G_{\text{OX}}^\circ$  and  $\Delta G_{\text{RED}}^\circ$ , respectively, are given by

$$\Delta G_{\text{OX}}^\circ = G_{\text{Cation}}^\circ - G_{\text{Neutral}}^\circ = -nFE_{\text{OX}}^{\text{FBA}} \quad (3)$$

$$\Delta G_{\text{RED}}^\circ = G_{\text{Anion}}^\circ - G_{\text{Neutral}}^\circ = -nFE_{\text{RED}}^{\text{FBA}} \quad (4)$$

since  $\Delta G^\circ = -nFE_{\text{redox}}^\circ$ . The redox free energies were converted to redox potentials (against NHE) as described in ref 17.

Table S.2 of the Supporting Information contains the parameters required to calculate the ground-state one-electron redox potentials for the FBAs in ACN and DMF. The calculated potentials are also recorded in Table 2 so a comparison with the experimental potentials can be made. The calculated oxidation potentials show virtually no variation with solvent, varying by a maximum of 0.2%. The reduction potentials showed a slightly larger variation of 1.1%. When water was used as the solvent, the redox potentials did not shift significantly (<100 mV, data not shown). ACN and DMF have very similar dielectric constants, so this agreement is not surprising given that the PCM model does not account for the specific interactions between solvent and solute.<sup>37-39</sup> The smaller than expected potential shift in water solvent highlights well-known deficiencies in the PCM model to account for hydrogen bonding.

On average, the pteridones 6MAP and DMAP have a higher oxidation potential than the pteridines 3MI and 6MI. Overall, the experimental values differ from the calculated values by less than 160 mV for all cases in both solvents. The pteridines have lower oxidation potentials than the pteridones, with the range spanning  $E_{\text{OX}}^{\circ\text{EXP}}(6\text{MAP}) = 1.95$  V compared to  $E_{\text{OX}}^{\circ\text{EXP}}(6\text{MI}) = 1.65$  V. Both pteridones and pteridines have higher oxidation potentials than 2AP.<sup>17</sup>

The reduction potentials for the pteridines/pteridones show poorer agreement between experimental and calculated values, so much so that the computations were not predictive for 6MI and 3MI due to the presence of two cathodic peaks in the (DMF) voltammograms. Taking the lowest potential cathodic peak,  $E_{\text{RED}}^{\circ\text{EXP}}$ , as a basis for comparison, the difference between experimental and calculated potentials is largest for 3MI (320 mV) and smallest for 6MAP (190 mV). One possible explanation for this behavior might be that the accuracy of the computed radical cation energy is better than that of the radical anion. However, a close comparison of the values in Table S.2 of the Supporting Information do not bear this out. A better explanation is that the multiplet structure of the cathodic CV makes the peak difficult to determine accurately without deconvolution. This is consistent with the larger spread in the difference between experiment and computation.

The differences between pteridine and pteridone reduction potentials are small. The largest difference is between 3MI and 6MI, about 240 mV. Interestingly, 6MAP, DMAP, and 3MI differ from each other by only 50 mV. All of these pteridone and pteridine analogues have lower reduction potentials than 2AP,<sup>17</sup> by as much as 700 mV.

**Excited-State Redox Potentials of the FBAs.** The excited-state oxidation and reduction potentials,  $E_{\text{OX}}^{\circ\text{FBA}^*}$  and  $E_{\text{RED}}^{\circ\text{FBA}^*}$ , can be calculated from the ground-state one-electron oxidation and reduction potentials reported in Table 2 according to the following equations:

$$E_{\text{OX}}^{\circ\text{FBA}^*} = E_{\text{OX}}^{\circ\text{FBA}} - E_{00} \quad (5)$$

$$E_{\text{RED}}^{\circ\text{FBA}^*} = E_{\text{RED}}^{\circ\text{FBA}} + E_{00} \quad (6)$$

Table 3 lists these potentials, as well as the  $E_{00}$  energies of the FBAs.  $E_{00}$  is the energy difference between the ground state and first excited electronic state obtained from the intersection of the normalized absorption and fluorescence emission spectra<sup>47</sup> of the FBAs in ACN or DMF for  $E_{\text{OX}}^{\circ\text{FBA}^*}$  and  $E_{\text{RED}}^{\circ\text{FBA}^*}$ , respectively. It should be pointed out that the excited-state potentials are about 0.1 V larger if the aqueous  $E_{00}$  energy is used instead of the  $E_{00}$  obtained in the solvent used for the CV measurements.

To our knowledge, the excited-state oxidation and reduction potentials of 6MAP, DMAP, 3MI, and 6MI have not been reported. The  $E_{\text{OX}}^{\circ\text{FBA}^*}$  values of these analogues are about 20% smaller than that for 2AP\* (~450 mV), while the  $E_{\text{RED}}^{\circ\text{FBA}^*}$  values of the analogues are about 30% larger than the corresponding value for 2AP\*.<sup>17</sup> In contrast, the excited-state oxidation potentials for these FBAs are within ~70 mV of each other. The excited-state reduction potentials,  $E_{\text{RED}}^{\circ}$ , of 6MAP, DMAP, and 3MI are approximately 1.89 V, within ~60 mV of each other. 6MI has a significantly lower potential of 1.41 V, about 400 mV lower than the other FBAs in this class. This difference has important consequences for the quenching rate constant of 6MI relative to the other FBAs. Inspection of Table 1 shows that 6MI does have the slowest quenching rate, in agreement with the excited-state potential calculated using the CV and spectroscopic results.

**Free Energy of Electron Transfer ( $\Delta G_{\text{ET}}^{\circ}$ ) for the Quenching of FBAs by Nucleic Acid Monophosphates.** The fluorescence quenching of FBAs by the nucleic acid monophosphate through electron transfer can happen through two possible scenarios. FBA\* can reduce the ground-state nucleic acid monophosphate (nucleobase reduction or NBR), or it can be reduced by the nucleic acid monophosphate (nucleobase oxidation or NBO). Which of these two processes happens depends on the free energy change. The free energy change for the electron transfer step ( $\Delta G_{\text{ET}}^{\circ}$ , ET = NBO or NBR) for both NBO and NBR can be calculated using the classic Rehm–Weller

**TABLE 3: Excited-State Oxidation and Reduction Potentials of FBAs<sup>a</sup>**

FBAs	$E_{00}$ (buffer)	$E_{00}$ (ACN)	$E_{00}$ (DMF)	$E_{\text{OX}}^{\circ\text{FBA}^*}$ (ACN)	$E_{\text{RED}}^{\circ\text{FBA}^*}$ (DMF)
6MAP	3.30	3.47	3.38	-1.52	1.92
DMAP	3.28	3.43	3.39	-1.55	1.89
3MI	3.23	3.29	3.27	-1.50	1.83
6MI	3.24	3.13	3.09	-1.48	1.41

<sup>a</sup>  $E_{00}$  is the energy (in eV) at the intersection of normalized absorption and the fluorescence emission spectra as measured in 0.1 M potassium phosphate buffer pH = 7.0, ACN, or DMF. The excited-state potentials for  $E_{\text{OX}}^{\circ\text{FBA}^*}$  and  $E_{\text{RED}}^{\circ\text{FBA}^*}$  are calculated using the  $E_{00}$  values for ACN and DMF, respectively. All values are in eV. The following oxidation/reduction potentials for the native bases are provided for comparison:<sup>31</sup>  $E_{\text{OX}}$  (G/A/C/T)  $\rightarrow$  1.49/1.96/2.14/2.11 V (in ACN);  $E_{\text{RED}}$  (G/A/C/T)  $\rightarrow$  < -2.76/-2.45/-2.23/-2.14 V (in DMF).

**TABLE 4: Free Energies of Electron Transfer ( $\Delta G_{\text{ET}}^{\circ}$ ) Calculated from the Rehm–Weller Equation (eqs 7–9) for the NBO ( $\Delta G_{\text{NBO}}^{\circ}$ ) and the NBR ( $\Delta G_{\text{NBR}}^{\circ}$ ) Schemes<sup>a</sup>**

FBA	NB	$\Delta G_{\text{NBO}}^{\circ}$	$\Delta G_{\text{NBR}}^{\circ}$
6MAP	G	-0.53	1.14
	A	-0.06	0.83
	C	0.12	0.61
	dT	0.09	0.52
DMAP	G	-0.50	1.11
	A	-0.03	0.80
	C	0.15	0.58
	dT	0.12	0.49
3MI	G	-0.44	1.16
	A	0.03	0.85
	C	0.21	0.63
	dT	0.18	0.54
6MI	G	-0.02	1.18
	A	0.45	0.87
	C	0.63	0.65
	dT	0.60	0.56

<sup>a</sup> The free energies, in eV, were calculated using data obtained in ACN or DMF for  $\Delta G_{\text{NBO}}^{\circ}$  or  $\Delta G_{\text{NBR}}^{\circ}$ , respectively.

equations:<sup>29</sup>

Nucleobase oxidation, NBO:

$$\Delta G_{\text{NBO}}^{\circ} = E_{\text{OX}}^{\circ\text{NB}} - E_{\text{RED}}^{\circ\text{FBA}^*} + \Delta G^{\circ}(\epsilon) \quad (7)$$

Nucleobase reduction, NBR:

$$\Delta G_{\text{NBR}}^{\circ} = E_{\text{OX}}^{\circ\text{FBA}^*} - E_{\text{RED}}^{\circ\text{NB}} + \Delta G^{\circ}(\epsilon) \quad (8)$$

where  $E_{\text{OX}}^{\circ\text{FBA}^*}$  and  $E_{\text{RED}}^{\circ\text{FBA}^*}$  are the excited-state oxidation and reduction potentials of the FBA, respectively,  $E_{\text{RED}}^{\circ\text{NB}}$  is the ground-state reduction potential of the nucleobase,  $E_{\text{OX}}^{\circ\text{NB}}$  is the ground-state oxidation potential of the nucleobase, and  $\Delta G^{\circ}(\epsilon)$  is the Born correction,

$$\Delta G^{\circ}(\epsilon) = \frac{e^2}{4\pi\epsilon_0} \left[ \left( \frac{1}{r_{\text{ion}}} - \frac{1}{r_{\text{EC}}} \right) \frac{1}{\epsilon_{\text{W}}} - \frac{1}{r_{\text{ion}}\epsilon_0} \right] \quad (9)$$

which accounts for the interaction energy between the two radical ions formed after electron transfer and helps account for the solvent change from an organic solvent whose dielectric constant is  $\epsilon_0$  to a solvent of interest  $\epsilon_{\text{W}}$ . In our case, the organic solvent is either acetonitrile or DMF and the solvent of interest is water. Using standard parameters for  $r_{\text{ion}} = 3.0 \text{ \AA}$  and  $r_{\text{EC}} = 7.0 \text{ \AA}$ , we obtain  $\Delta G^{\circ}(\epsilon) \sim -0.1 \text{ eV}$ .<sup>31</sup>

The calculated  $\Delta G_{\text{ET}}^{\circ}$  values for NBO and NBR are listed in Table 4. All values are positive with the exception of  $\Delta G_{\text{NBO}}^{\circ}$  for GMP. For the pteridines,  $\Delta G_{\text{NBR}}^{\circ} > \Delta G_{\text{NBO}}^{\circ}$  by at least 0.35 eV and as much as 1.8 V, except for the case of 6MI with CMP.

If the free energy of contribution from water solvation stabilizes the complex, the resulting decrease in  $\Delta G_{\text{ET}}^{\circ}$  could support electron transfer quenching. This must be the case because quenching is efficient for AMP and both CMP and TMP quench to varying extents as well. The Born correction is not large enough to produce negative free energies for all FBAs in water. This raises the question as to whether hydrogen bonding plays a special role in the fluorescence quenching of these FBAs. We have shown this to be the case for 2AP.<sup>17</sup>

Examination of  $\Delta G_{\text{NBO}}^{\circ}$  and  $\Delta G_{\text{NBR}}^{\circ}$  for 6MI suggests that 6MI could undergo both NBO or NBR by C and dT, as these NMPs have free energies in the same range, about 0.6 eV (see Table

4). However, such a large positive free energy will not be a spontaneous ET process and it is unlikely that the free energy shift obtained in going from organic solvent to water will make it so. This is borne out in the analysis below. If PET from pyrimidines is eliminated, then it is no longer possible to fit the quenching data for 6MI to obtain a unique  $\Delta G_{\text{ET}}^{\circ}$  and  $\lambda_0$  simply because there are too few data points left.

**Calculation of the Free Energy Shift in Aqueous Solutions ( $\Delta G_{\text{q}}^{\circ}$ ) and Solvent Reorganization Energy ( $\lambda_0$ ).** The total free energy of quenching  $\Delta G_{\text{q}}^{\circ}$  can be expressed as the sum of  $\Delta G_{\text{ET}}^{\circ}$  and  $\Delta G_{\text{W}}^{\circ}$ :

$$\Delta G_{\text{q}}^{\circ} = \Delta G_{\text{ET}}^{\circ} + \Delta G_{\text{W}}^{\circ} \quad (10)$$

The value of  $\Delta G_{\text{W}}^{\circ}$  and the corresponding solvent reorganization energy,  $\lambda_0$ , for each FBA are not known and have to be determined from a fit of the fluorescence quenching constant  $k_{\text{q}}$  to  $\Delta G_{\text{ET}}^{\circ}$  according to the Scandola–Balzani (S–B) equation:<sup>48</sup>

$$k_{\text{q}} = \frac{k_{\text{d}}}{1 + \frac{k_{\text{d}}}{\nu_{\text{N}} K_{\text{A}}} \left[ \exp\left(\frac{E^{\ddagger}}{RT}\right) + \exp\left(\frac{\Delta G_{\text{q}}^{\circ}}{RT}\right) \right]} \quad (11)$$

where

$$E^{\ddagger} = \Delta G_{\text{q}}^{\circ} + \frac{\lambda_0}{4 \ln(2)} \ln \left\{ 1 + \exp \left[ -\frac{\Delta G_{\text{q}}^{\circ} \ln(2)}{\lambda_0/4} \right] \right\} \quad (12)$$

and  $k_{\text{d}}$  is the diffusion rate constant and the equilibrium constant for the association of the encounter complex,  $K_{\text{A}} = k_{\text{d}}/k_{-\text{d}}$ . Here,  $k_{-\text{d}}$  is the dissociation rate constant for the encounter complex.  $\nu_{\text{N}}$  is the frequency factor for a bimolecular reaction in solution, and  $T$  is the temperature. Since the values of  $\nu_{\text{N}}$  and  $k_{-\text{d}}$  were not known, they were fitted as a single pre-exponential factor

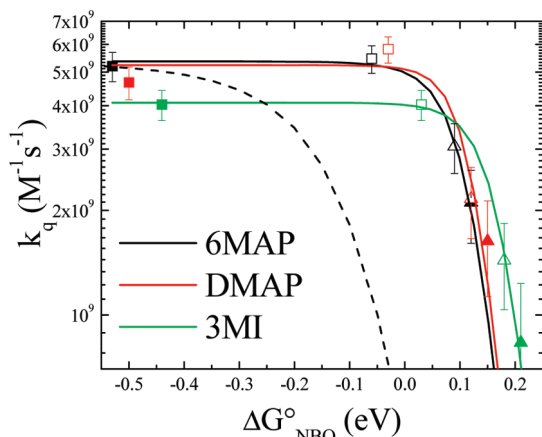


**Figure 4.** Plot of  $k_{\text{q}}$  against  $\Delta G_{\text{NBO}}^{\circ}$  for the FBAs 6MAP, DMAP, and 3MI. Square symbols are purines, and triangular symbols are pyrimidines (GMP = ■, AMP = □, CMP = ▲, TMP = △). The error bars are derived from a propagation of errors treatment using the standard deviation in the fitted parameters. The lines are the computed quenching curves based on the method of Scandola and Balzani.<sup>48</sup> During the fitting procedure,  $k_{\text{d}}$  was held constant at  $6.79 \times 10^9 \text{ M}^{-1} \text{ s}^{-1}$ . A calculation of  $k_{\text{q}}$  for 6MAP using  $\lambda_0 = 0.4 \text{ eV}$  (—) shows the sensitivity of the Scandola–Balzani function to  $E_{\text{NBO}}^{\ddagger}$ .

**TABLE 5: The Parameters for eq 13 Were Obtained by Simultaneously Fitting  $k_{\text{q}}$  against  $\Delta G_{\text{NBO}}^{\circ}$  for 6MAP, DMAP, and 3MI; during the Fitting Procedure,  $k_{\text{d}}$  Was Held Constant; the Errors Shown in the Table Are the Errors from the Fitting Procedure**

FBA	$\alpha$	$\Delta G_{\text{W}}^{\circ}$ (eV)	$\lambda_0$ (eV)
6MAP	$0.27 \pm 0.10$	$-0.10 \pm 0.04$	$0.15 \pm 0.15$
DMAP	$0.30 \pm 0.10$	$-0.11 \pm 0.03$	$0.11 \pm 0.18$
3MI	$0.66 \pm 0.15$	$-0.17 \pm 0.03$	$0.13 \pm 0.14$

**TABLE 6: Table Showing the Sum of Free Energy of Electron Transfer  $\Delta G_{\text{NBO}}^{\circ}$  and the Free Energy Shift in Aqueous Solution  $\Delta G_{\text{W}}^{\circ}$  and the Solvent Reorganization Energy ( $\lambda_0$ )<sup>a</sup>**

FBA	NB	$\Delta G_{\text{NBO}}^{\circ} + \Delta G_{\text{W}}^{\circ}$	$E_{\text{NBO}}^{\ddagger}$ (eV)
6MAP	G	-0.63	0.000
	A	-0.16	0.003
	C	0.021	0.048
	dT	-0.009	0.032
DMAP	G	-0.61	0.000
	A	-0.14	0.001
	C	0.045	0.055
	dT	0.015	0.035
3MI	G	-0.61	0.000
	A	-0.14	0.002
	C	0.037	0.053
	dT	0.007	0.0353

<sup>a</sup> The activation energy,  $E_{\text{NBO}}^{\ddagger}$ , is also shown. For comparison, the thermal energy available at 293 K is  $3/2k_{\text{B}}T \sim 0.038 \text{ eV}$ . All values are in eV.

$$E_{\text{NBO}}^{\ddagger} = \Delta G_0' + \frac{\lambda_0}{4 \ln(2)} \ln \left\{ 1 + \exp \left[ -\frac{\Delta G_0' \ln(2)}{\lambda_0/4} \right] \right\},$$

where  $\Delta G_0' = \Delta G_{\text{NBO}}^{\circ} + \Delta G_{\text{W}}^{\circ}$

$\alpha = k_{-\text{d}}/\nu_{\text{N}}$ .  $k_{\text{d}}$  was set to  $6.79 \times 10^9 \text{ M}^{-1} \text{ s}^{-1}$  at 293 K based on the Smoluchowski equation.

The values of  $\Delta G_{\text{q}}^{\circ}$ ,  $\lambda_0$ , and  $\alpha$  were obtained for each individual FBA by a nonlinear fit of  $k_{\text{q}}$  against  $\Delta G_{\text{ET}}^{\circ}$  based on eq 11. Care was taken to ensure that the fitted results were not sensitive to the starting parameters. The free parameters were fitted with and without constraints ( $-1.50 \text{ eV} \leq \Delta G_{\text{W}}^{\circ} \leq 0.10 \text{ eV}$  and  $0.0 \text{ eV} \leq \lambda_0 \leq 1.2 \text{ eV}$ ). The fitted S–B curves and parameters are shown in Figure 4 and Table 5. Fitting the data to the NBR scheme gave physically unreasonable values for  $\Delta G_{\text{W}}^{\circ}$  and  $\lambda_0$  in either case. For NBR to be thermodynamically spontaneous,  $\Delta G_{\text{W}}^{\circ}$  values will have to be more negative than those required for NBO, in some cases by as much as 1 eV. Such high free energy shifts do not seem to be supportable on the basis of the work of Seidel et al.<sup>31</sup>

Fitting the data using the  $\Delta G_{\text{NBO}}^{\circ}$  values gave physically reasonable parameters for 6MAP, DMAP, and 3MI with or without constraints. The values of  $\Delta G_{\text{W}}^{\circ}$  vary from about  $-0.1 \text{ eV}$  for the pteridones to  $-0.17 \text{ eV}$  for 3MI. This difference might be due to the slightly higher hydrogen bonding ability of pteridones over pteridones.  $\lambda_0$  is in the range of about 0.14 eV. Using the fitted parameters, it can be seen from Table 6 that the free energy for electron transfer is negative (or nearly so) for GMP, AMP, and dTMP. Where the free energy is positive (e.g., 0.045 eV for DMAP:CMP), the endothermicity is small compared to thermal energy (about 0.038 eV at 293 K). Thus, quenching through NBO appears reasonable by all PTERS except 6MI. This assignment does not rule out quenching by other mechanisms, but a comparison of the calculated activation energies with the trend in  $k_{\text{q}}$  supports this view (*vide infra*),

and a good fit to the Scandola–Balzani equation would not be expected if ET were not the dominant quenching mechanism.

An example of the sensitivity of the S–B equation to the activation energy,  $E_{\text{NBO}}^{\ddagger}$  (eq 12), is shown in Figure 4 as a dashed black line for 6MAP. Here,  $E_{\text{NBO}}^{\ddagger}$  was recalculated using  $\lambda_0 = 0.4$  eV instead of the fitted value of 0.15 eV. The function deviates strongly from the data and, as expected, approaches the diffusion limit at  $\Delta G_{\text{NBO}}^{\circ} < -0.4$  eV. Because of the somewhat low reorganization energy retrieved, we refitted the 6MAP data set constraining the reorganization energy to be above 0.4 eV. The resulting  $\Delta G_{\text{W}}^{\circ}$ ,  $\lambda_0$ , and  $\alpha$  parameters were  $-0.2$  eV, 0.4 eV, and 0.16, respectively. These are not unreasonable values, but the fit, however, was about 10 times more worse based on a comparison of the respective  $\chi^2$  values.

6MAP and DMAP have nearly identical values of  $\alpha$ ,  $\Delta G_{\text{W}}^{\circ}$ , and  $\lambda_0$ , as might be expected on the basis of their chemical similarity. The  $\alpha$  parameter for 3MI is about 2 times larger than that for 6MAP and DMAP. If we presume that the collision frequency,  $\nu_{\text{N}}$ , is similar for all PTERs, then the difference in  $\alpha$  for 3MI must due to  $k_{-\text{d}}$ , suggesting that the dissociation constants for the 3MI\*:NMP complexes are larger than those for the pteridones. This would lead to a shorter reaction time for electron transfer, which is consistent with the lower  $k_{\text{q}}$  values obtained for 3MI.

## Discussion

**Steady-State Fluorescence Quenching of FBAs.** On the basis of the excellent agreement of our quenching data with the free energy of nucleobase oxidation, we think that PET is the dominant mechanism for excited-state quenching in 6MAP, DMAP, and 3MI. 6MI also appears to undergo PET quenching, at least for GMP and possibly for AMP. Quenching by the pyrimidines appears to be energetically less favorable, and perhaps competing quenching pathways dominate. Our thermodynamic data are consistent with what has been reported for all PTERs when they are incorporated in single- and double-stranded DNA,<sup>18,20</sup> with the exception of 6MI.<sup>24,49</sup>

Generally, the FBAs showed the greatest quenching by purine monophosphates, even when complexation was taken into account. However, to definitively assign these results to photoinduced electron transfer, we must first rule out other de-excitation pathways. Quenching cannot occur through Förster type energy transfer because there is no overlap between the donor ( $\text{D}^*$ ) emission spectra and the acceptor (A) absorption spectra. This leaves Dexter energy transfer, intersystem crossing, exciplex formation, or quenching through a conical intersection as possible dark mechanisms. These mechanisms are fast enough to compete with radiative decay or PET if the D–A distance,  $r_{\text{DA}}$ , is small.

Dexter transfer, an electron exchange mechanism, is efficient for small donor–acceptor separations,  $r_{\text{DA}} \sim 3\text{--}7$  Å, where orbital overlap between the donor and acceptor becomes appreciable.<sup>50</sup> In this mechanism, energy transfer results because of electron exchange between  $\text{D}^*$  and A as a result of which  $\text{A} \rightarrow \text{A}^*$  and  $\text{D}^* \rightarrow \text{D}$ . Fluorescence quenching is possible through this mechanism only if the energy difference in going from D to  $\text{D}^*$  matches the energy difference in going from A to  $\text{A}^*$ . For the FBAs and NMPs used in this study, Dexter energy transfer can be ruled out because of the absence of energy matching.<sup>26,50,51</sup>

Intersystem crossing,  $^1\text{FBA}^* \rightarrow ^3\text{FBA}^*$ , can be a possible quenching mechanism. Triplet formation should result in weak phosphorescence. We did not observe any long wavelength emission growing in as a function of NMP concentration; thus,

it is unlikely that intersystem crossing contributes to the observed quenching. Likewise, FBA fluorescence could be quenched due to the formation of exciplexes,<sup>52</sup> but this should also lead to weak red-shifted emission. We were unable to find evidence for this in our fluorescence data.

Charge transfer quenching spans two regimes: full electron transfer resulting in a pair of radical ions and “partial” charge transfer, in which the excited-state donor forms an excited-state charge transfer complex (CTC<sup>53</sup>) with the acceptor. Photoinduced electron transfer (PET) can occur over large  $r_{\text{DA}}$  depending on the electronic coupling between the donor and acceptor, the driving force, and the reorganization energy. CTCs are readily formed and can lead to quenching, as the CT states often have very low transition dipole moments and consequently low radiative rates. CTCs often show a CT band well to the red of the donor absorption band. We have not seen any indication that such a band exists, even at the highest quencher concentrations.

Finally, it is possible that complex formation engenders a conical intersection<sup>54–58</sup> on the potential surface of excited FBA that is absent for the FBA alone. The result of a CI in the complex should be an ultrafast excited state  $\rightarrow$  ground state transition. Unfortunately, there is no spectroscopic signature of this mechanism that is accessible based on the steady-state methods employed in this study. However, it would be very unusual to obtain the correlation with redox potentials seen here if the CI mechanism were invoked. Therefore, we conclude that PET is the likely quenching mechanism. However, definitive evidence could be obtained by the observation of the transient radical ions involved.

**Pteridine/Pteridone Quenching.** A study of the quenching of the methylated free base of 6MI using KI was performed by Seibert et al.<sup>42</sup> They observed  $k_{\text{q}} = 6.74 \times 10^9 \text{ M}^{-1} \text{ s}^{-1}$ , in excellent agreement with what we calculated as the diffusion-limited rate constant. Because iodide ion is much smaller than the NMPs, this result provides a good checkpoint for our results.  $k_{\text{q}}$  values higher than this would be suspicious.

The quenching patterns of the NMPs with 6MAP, DMAP, and 3MI are consistent with earlier observations by Hawkins et al.<sup>24</sup> for these FBAs incorporated into single- and double-stranded DNA. A study of 3MI and 6MI quenching was published recently by Poulin et al.<sup>49</sup> which showed a similar quenching pattern observed here. These studies also used a combination of S–V kinetics and time-resolved fluorescence spectroscopy to ascertain the degree of static quenching due to the presence of ground-state complexes. The dynamic S–V constants given in that work (with the exception of thymidine) are 6MI  $K_{\text{d}} (\text{M}^{-1}) = 17/13/3.3$  and 3MI  $K_{\text{d}} (\text{M}^{-1}) = 17/15/7.2$  for G/A/C, respectively. The agreement for 6MI is fair, within a factor of 2, while agreement with their 3MI results is somewhat better. The largest technical difference in the studies is the method in which the static quenching contribution was ascertained. We used steady-state data and the modified S–V equation, while Poulin et al. relied more heavily on time-resolved emission to obtain the constants.

Generally speaking, time-resolved emission should give more reliable information<sup>26</sup> about the quenching constants, particularly when ground-state complexation can lead to nonemissive states. However, our time-resolved studies for 6MI:CMP show no quenching (Figure 2), while the Knutson group saw evidence of quenching in their time-correlated single photon counting studies. Indeed, the slope of a plot of 6MI lifetimes  $\tau_0/\tau$  vs [CMP] gave a value close to that for the steady-state result ( $1.2$  vs  $1.7 \text{ M}^{-1}$ , Table 1 and Figure S1 of the Supporting Informa-

tion). Both time-resolved studies show significant static quenching of the 6MI:GMP complex. We retrieved a linear  $\tau_0/\tau$  vs [GMP] relationship for 6MI:GMP which was within 25% of the steady-state value (9.5 vs 12.1 M<sup>-1</sup>, respectively). Poulin et al. obtained a nonlinear relationship between [GMP] and  $\tau_0/\tau$  in their study. We cannot, at present, account for this discrepancy.

It is interesting to note that the total electron transfer free energy for quenching by guanine through NBO is significantly more negative than adenine. However, the degree of quenching by AMP is about the same or greater than GMP for all four FBAs (see Table 1 and Figure 1). This could be due to differences in the  $k_{-d}$  between the donor–acceptor pairs. From the current analysis, it is not possible to extract information about  $k_{-d}$  from  $\alpha$  for the individual donor–acceptor pairs, because these interactions are averaged together in the fit.

The activation energies for the electron transfer process based on eq 12 have been tabulated in Table 6. The quenching of 6MAP\*, DMAP\*, and 3MI\* by GMP appears to be activationless. This can be attributed to the low oxidation potential of guanine (1.49 V vs NHE) compared to the other native bases. However, quenching by AMP has a minimal barrier. The actual difference between these calculated activation energies and our observed quenching propensities may be the result of small experimental errors, not only in our values but potentially the redox values used for the NMPs, which have error bars of  $\pm 0.05$  V.<sup>31</sup> Our results do provide a satisfying justification for the slightly higher quenching propensity of dT over C, because  $E_{\text{NBO}}^{\text{r}}(\text{CMP})$  is about 20 meV larger than  $E_{\text{NBO}}^{\text{r}}(\text{TMP})$ . A measurement of the temperature dependence of quenching should be informative about whether guanine oxidation by PTER\* is truly activationless.

A major uncertainty concerning the application of this study to base-stacked helical DNA or RNA has to do with the geometrical arrangement of the complex. From the 1960s, it has been shown that monomer bases form stacked complexes and do not engage in WC base pairing.<sup>59</sup> However, if solvation of these dipolar molecules is ignored, simple electrostatics predicts that the most stable encounter complex would have a relatively noncoplanar but staggered “head-to-tail” alignment of the FBA with the NB, with stabilization on the order of  $-1$  eV.<sup>60</sup> Compared to this, a stacked “head-to-tail” geometry has a much weaker stabilization energy,  $\sim 0.25$  eV. However, solvation in water shields the dipoles so that  $\pi$ -stacking appears to be the dominant interaction. Stacking must inevitably lead to a loss of solvent between the molecules, and it may be that the intrinsic dipoles exert some degree of orientation on the stack. Of course, steric hindrance plays a role as well, especially in the case of the NMPs, which all have ribose–phosphate side chains.

The solvent reorganization energies,  $\lambda_0$ , from the fits are significantly lower than the frequently used value of  $\sim 1$  eV, as reported for 2AP.<sup>13</sup> This estimate was based on the outer sphere reorganization energy for spherical reactants and a net zero initial dipole moment of the donor–acceptor pair before electron transfer.<sup>61</sup> The pteridines/pteridones are molecules which have large permanent ground-state dipole moments. The alignment of these dipole moments upon formation of the (transient) encounter complex should have a significant effect on  $\lambda_0$ . As discussed above, for dipole–dipole interactions, the lowest energy is achieved for a “staggered head-to-tail” geometry.<sup>60</sup> Assuming this is the geometry of the encounter complex, the net change in dipole moment due to electron transfer ( $\text{D}-\text{A} \rightarrow \text{D}^+-\text{A}^-$ , where  $\text{D} = \text{NB}$  and  $\text{A} = \text{FBA}$ ) is the important factor in determining  $\lambda_0$ . For example, Eberson has tabulated many

cases of self-exchange reactions where  $\lambda_0 < 1$  eV.<sup>30</sup> Nonetheless, we recognize that the reorganization energies reported here may be in error by several tenths of electronvolts.

It is interesting that the excited-state reduction potentials of 2AP<sup>17</sup> and 6MI are essentially equal (1.44 vs 1.41 eV, respectively). However, 2AP\* can undergo electron transfer with pyrimidines by oxidation ( $E_{\text{OX}}^{\text{e}2\text{AP}^*} = -2.03$  eV<sup>17</sup>), a path that is thermodynamically unfavorable for 6MI ( $E_{\text{OX}}^{\text{e}6\text{MI}^*} = -1.48$  eV), which shows no quenching by pyrimidines. Thus, 6MI may be a more selective FBA than 2AP, principally because of its insensitivity to thymine and cytosine. The ability to swap 6MI and 3MI in the same sequences may afford a differential sensitivity to the 5' or 3' bases surrounding the pteridine FBA. In this regard, 6MAP and DMAP appear to be indistinguishable. However, the slightly higher activation energies that DMAP exhibits for pyrimidines may be exploited by varying the temperature of the system.

A final caveat is that the geometry of the encounter complexes in solution might be very different from base-stacked FBAs in oligonucleotides. Nonetheless, the excited-state redox potentials determined in this study represent the essential first step in understanding and exploiting PET in DNA/RNA decorated with these FBAs. Without these values, it would be difficult to properly assign changes in fluorescence intensity from these FBAs when studying DNA/RNA binding proteins, or in utilizing the PTERS in, for example, molecular beacons or in DNA photonic materials.

## Conclusions

The central theme of this work has been to determine whether fluorescence quenching by photoinduced electron transfer in PTER:NMP complexes is thermodynamically feasible and whether the PTER acts as an excited-state donor or acceptor. The results from the steady-state quenching and electrochemistry experiments suggest that 6MAP\*, DMAP\*, and 3MI\* act as excited-state acceptors and are preferentially quenched by purines. 6MI\* acts as an acceptor but is quenched by purines only.

To our knowledge, we have presented the first measurements and calculations of one-electron oxidation and reduction potentials of these pteridine/pteridone FBAs in aprotic organic solvents. On the basis of the experimental ground-state redox potentials, their excited-state redox potentials were obtained. These excited-state potentials were used in the Rehm–Weller equation to calculate free energies of electron transfer,  $\Delta G_{\text{ET}}^{\text{e}}$ , for these FBAs. Aqueous solvation was critical in tuning the free energy via  $\Delta G_{\text{W}}^{\text{e}}$  to obtain spontaneous electron transfer. The calculated activation energy for each donor–acceptor pair was successfully able to account for the observed quenching patterns. The reorganization energies found for these FBA:NMP pairs were significantly lower than commonly reported for molecules of this kind.

**Acknowledgment.** We wish to thank Dr. Eric Borguet, Department of Chemistry, Temple University, for access to his potentiostat and for useful discussions. M.N. would like to thank Mr. Venkat Velvadapu of Dr. Rodrigo Andrade's research group, Department of Chemistry, Temple University. M.N. and R.J.S. would like to thank Dr. Vincent Rotello at the University of Massachusetts at Amherst and Dr. Anthony Addison at Drexel University for their valuable input on the CV results. Jay Knutson (NIH) and David Beratan (Duke University) provided useful conversations about the quenching results. M.N. was supported, in part, by NSF grant CHE-0847855. This research

was supported in part by Grant No. MCB080057P from the Pittsburgh Supercomputer Center, supported by several federal agencies, the Commonwealth of Pennsylvania, and private industry.

**Supporting Information Available:** Complete ref 35, tables of 6MI and 6MAP lifetimes, table of calculated one-electron oxidation/reduction potentials of methylated FBAs, and graph of the ratio of lifetimes vs [NMP] for 6MI and 6MAP. This material is available free of charge via the Internet at <http://pubs.acs.org>.

## References and Notes

- (1) Wilson, J. N.; Kool, E. T. Fluorescent DNA base replacements: reporters and sensors for biological systems. *Org. Biomol. Chem.* **2006**, *4*, 4265–4274.
- (2) Kool, E. T. Replacing the Nucleobases in DNA with Designer Molecules. *Acc. Chem. Res.* **2002**, *35*, 936–943.
- (3) Christine, K. S.; MacFarlane, A. W., IV; Yang, K.; Stanley, R. J. Cyclobutylpyrimidine Dimer Base Flipping by DNA Photolyase. *J. Biol. Chem.* **2002**, *277*, 38339–38344.
- (4) Guest, C. R.; Hochstrasser, R. A.; Sowers, L. C.; Millar, D. P. Dynamics of mismatched base pairs in DNA. *Biochemistry* **1991**, *30*, 3271–3279.
- (5) Ha, T. Single-molecule fluorescence methods for the study of nucleic acids. *Curr. Opin. Struct. Biol.* **2001**, *11*, 287–292.
- (6) Hariharan, C.; Reha-Krantz, L. J. Using 2-Aminopurine Fluorescence To Detect Bacteriophage T4 DNA Polymerase-DNA Complexes That Are Important for Primer Extension and Proofreading Reactions. *Biochemistry* **2005**, *44*, 15674–15684.
- (7) Hawkins, M. E. Fluorescent pteridine nucleoside analogs. A window on DNA interactions. *Cell Biochem. Biophys.* **2001**, *34*, 257–281.
- (8) Yang, K.; Matsika, S.; Stanley, R. J. 6MAP, a fluorescent adenine analogue, is a probe of base flipping by DNA photolyase. *J. Phys. Chem. B* **2007**, *111*, 10615–10625.
- (9) Yang, K.; Stanley, R. J. Differential Distortion of Substrate Occurs When It Binds to DNA Photolyase: A 2-Aminopurine Study. *Biochemistry* **2006**, *45*, 11239–11245.
- (10) Yang, K.; Stanley, R. J. The extent of DNA deformation in DNA photolyase-substrate complexes: A solution state fluorescence study. *Photochem. Photobiol.* **2008**, *84*, 741–749.
- (11) Tinsley, R. A.; Walter, N. G. Pyrrolo-C as a fluorescent probe for monitoring RNA secondary structure formation. *RNA* **2006**, *12*, 522–529.
- (12) Ward, D. C.; Reich, E.; Stryer, L. Fluorescence studies of nucleotides and polynucleotides. I. Formycin, 2-aminopurine riboside, 2,6-diaminopurine riboside, and their derivatives. *J. Biol. Chem.* **1969**, *244*, 1228–1237.
- (13) Fiebig, T.; Wan, C.; Zewail, A. H. Femtosecond charge transfer dynamics of a modified DNA base: 2-aminopurine in complexes with nucleotides. *ChemPhysChem* **2002**, *3*, 781–788.
- (14) Larsen, O. F. A.; van Stokkum, I. H. M.; de Weerd, F. L.; Vengris, M.; Aravindakumar, C. T.; van Grondelle, R.; Geacintov, N. E.; van Amerongen, H. Ultrafast transient-absorption and steady-state fluorescence measurements on 2-aminopurine substituted dinucleotides and 2-aminopurine substituted DNA duplexes. *Phys. Chem. Chem. Phys.* **2003**, *6*, 154–160.
- (15) Larsen, O. F. A.; van Stokkum, I. H. M.; de Weerd, F. L.; Vengris, M.; Aravindakumar, C. T.; van Grondelle, R.; Geacintov, N. E.; van Amerongen, H. Ultrafast transient-absorption and steady-state fluorescence measurements on 2-aminopurine substituted dinucleotides and 2-aminopurine substituted DNA duplexes. *Phys. Chem. Chem. Phys.* **2004**, *6*, 154–160.
- (16) Somsen, O. J. G.; Van Hoek, A.; Van Amerongen, H. Fluorescence quenching of 2-aminopurine in dinucleotides. *Chem. Phys. Lett.* **2005**, *402*, 61–65.
- (17) Narayanan, M.; Kodali, G.; Xing, Y.; Stanley, R. J. Photoinduced electron transfer occurs between 2-aminopurine and the DNA nucleic acid monophosphates: results from cyclic voltammetry and fluorescence quenching. *J. Phys. Chem. B*, submitted for publication, **2010**.
- (18) Hawkins, M. E.; Pfeleiderer, W.; Jungmann, O.; Balis, F. M. Synthesis and Fluorescence Characterization of Pteridine Adenosine Nucleoside Analogs for DNA Incorporation. *Anal. Biochem.* **2001**, *298*, 231–240.
- (19) Kenfack, C. A.; Burger, A.; Mély, Y. Excited-State Properties and Transitions of Fluorescent 8-Vinyl Adenosine in DNA. *J. Phys. Chem. B* **2006**, *110*, 26327–26336.
- (20) Driscoll, S. L.; Hawkins, M. E.; Balis, F. M.; Pfeleiderer, W.; Laws, W. R. Fluorescence properties of a new guanosine analog incorporated into small oligonucleotides. *Biophys. J.* **1997**, *73*, 3277–3286.
- (21) Berry, D. A.; Jung, K.-Y.; Wise, D. S.; Sercel, A. D.; Pearson, W. H.; Mackie, H.; Randolph, J. B.; Somers, R. L. Pyrrolo-dC and pyrrolo-C: fluorescent analogs of cytidine and 2'-deoxycytidine for the study of oligonucleotides. *Tetrahedron Lett.* **2004**, *45*, 2457–2461.
- (22) Nordlund, T. M.; Wu, P.; Andersson, S.; Nilsson, L.; Rigler, R.; Graeslund, A.; McLaughlin, L. W.; Gildea, B. Structural dynamics of DNA sensed by fluorescence from chemically modified bases. *Proc. SPIE* **1990**, *1204*, 344–353.
- (23) Wu, P.; Nordlund, T. M.; Gildea, B.; McLaughlin, L. W. Base stacking and unstacking as determined from a DNA decamer containing a fluorescent base. *Biochemistry* **1990**, *29*, 6508–6514.
- (24) Hawkins, M. E.; Pfeleiderer, W.; Balis, F. M.; Porter, D.; Knutson, J. R. Fluorescence properties of pteridine nucleoside analogs as monomers and incorporated into oligonucleotides. *Anal. Biochem.* **1997**, *244*, 86–95.
- (25) Hawkins, M. E. Synthesis, purification and sample experiment for fluorescent pteridine-containing DNA: tools for studying DNA interactive systems. *Nat. Protoc.* **2007**, *2*, 1013–1021.
- (26) Lakowicz, J. R. *Principles of Fluorescence Spectroscopy*, 3rd ed.; Springer: New York, 2006.
- (27) Marcus, R. A. On the theory of oxidation reduction reactions involving electron transfer. I\*. *J. Chem. Phys.* **1956**, *24*, 966–978.
- (28) Marcus, R. A.; Sutin, N. Electron transfers in chemistry and biology. *Biochim. Biophys. Acta* **1985**, *811*, 265–322.
- (29) Rehm, D.; Weller, A. Kinetics of Fluorescence Quenching by Electron and H-Atom Transfer. *Isr. J. Chem.* **1970**, *8*, 259–271.
- (30) Ebersson, L. Electron-transfer reactions in organic chemistry. *Adv. Phys. Org. Chem.* **1982**, *18*, 79–185.
- (31) Seidel, C. A. M.; Schulz, A.; Sauer, M. H. M. Nucleobase-Specific Quenching of Fluorescent Dyes. I. Nucleobase One-Electron Redox Potentials and Their Correlation with Static and Dynamic Quenching Efficiencies. *J. Phys. Chem.* **1996**, *100*, 5541–5553.
- (32) Cavaluzzi, M. J.; Borer, P. N. Revised UV extinction coefficients for nucleoside-5'-monophosphates and unpaired DNA and RNA. *Nucleic Acids Res.* **2004**, *32*, 1–9.
- (33) Sanabia, J. E.; Goldner, L. S.; Lacaze, P.-A.; Hawkins, M. E. On the Feasibility of Single-Molecule Detection of the Guanosine Analogue 3-MI. *J. Phys. Chem. B* **2004**, *108*, 15293–15300.
- (34) Melguizo, M.; Gottlieb, M.; Charubala, R.; Pfeleiderer, W. Nucleosides. LXII. Synthesis of 6-Methyl-8-(2-deoxy- $\beta$ -D-ribofuranosyl)-isoxanthopterin and Derivatives. *Nucleosides, Nucleotides Nucleic Acids* **1998**, *17*, 175–186.
- (35) Frisch, M. J.; et al. *Gaussian 03*, revision A.1; Gaussian, Inc.: Pittsburgh, PA, 2003.
- (36) Böes, E. S.; Livotto, P. R.; Stassen, H. Solvation of monovalent anions in acetonitrile and N, N-dimethylformamide: Parameterization of the IEF-PCM model. *Chem. Phys.* **2006**, *331*, 142–158.
- (37) Miertus, S.; Scrocco, E.; Tomasi, J. Electrostatic interaction of a solute with a continuum. A direct utilization of AB initio molecular potentials for the prevision of solvent effects. *Chem. Phys.* **1981**, *55*, 117–129.
- (38) Miertus, S.; Tomasi, J. Approximate evaluations of the electrostatic free energy and internal energy changes in solution processes. *Chem. Phys.* **1982**, *65*, 239–245.
- (39) Pascual-Ahuir, J. L.; Silla, E.; Tomasi, J.; Bonaccorsi, R. Electrostatic interaction of a solute with a continuum. Improved description of the cavity and of the surface cavity bound charge distribution. *J. Comput. Chem.* **2004**, *8*, 778–787.
- (40) Lorente, C.; Capparelli, A. L.; Thomas, A. H.; Braun, A. M.; Oliveros, E. Quenching of the fluorescence of pterin derivatives by anions. *Photochem. Photobiol. Sci.* **2004**, *3*, 167–173.
- (41) Stivers, J. T. 2-Aminopurine fluorescence studies of base stacking interactions at abasic sites in DNA: metal-ion and base sequence effects. *Nucleic Acids Res.* **1998**, *26*, 3837–3844.
- (42) Seibert, E.; Chin, A. S.; Pfeleiderer, W.; Hawkins, M. E.; Laws, W. R.; Osman, R.; Ross, J. B. A. pH-Dependent Spectroscopy and Electronic Structure of the Guanine Analogue 6,8-Dimethylisoxanthopterin. *J. Phys. Chem. A* **2003**, *107*, 178–185.
- (43) Petroselli, G.; Dantola, M. L.; Cabrerizo, F. M.; Lorente, C.; Braun, A. M.; Oliveros, E.; Thomas, A. H. Quenching of the Fluorescence of Aromatic Pterins by Deoxynucleotides. *J. Phys. Chem. A* **2009**, *113*, 1794–1799.
- (44) Kelley, S. O.; Barton, J. K. Electron transfer between bases in double helical DNA. *Science (Washington, DC, U. S.)* **1999**, *283*, 375–381.
- (45) Bharill, S.; Sarkar, P.; Ballin, J. D.; Gryczynski, I.; Wilson, G. M.; Gryczynski, Z. Fluorescence intensity decays of 2-aminopurine solutions: Lifetime distribution approach. *Anal. Biochem.* **2008**, *377*, 141–149.
- (46) Pandey, A.; Datta, S. N. Theoretical Determination of Standard Oxidation and Reduction Potentials of Chlorophyll-a in Acetonitrile. *J. Phys. Chem. B* **2005**, *109*, 9066–9072.
- (47) Kavarnos, G. J. *Fundamentals of Photoinduced Electron Transfer*; VCH Publishers: New York, 1993.

- (48) Scandola, F.; Balzani, V. Free-energy relationships for electron-transfer processes. *J. Am. Chem. Soc.* **1979**, *101*, 6140–6142.
- (49) Poulin, K. W.; Smirnov, A. V.; Hawkins, M. E.; Balis, F. M.; Knutson, J. R. Conformational Heterogeneity and Quasi-Static Self-Quenching in DNA Containing a Fluorescent Guanine Analogue, 3MI or 6MI. *Biochemistry* **2009**, *48*, 8861–8868.
- (50) Dexter, D. L. A theory of sensitized luminescence in solids. *J. Chem. Phys.* **1953**, *21*, 836–850.
- (51) Scoles, G. D.; Ghiggino, K. P. Electronic interactions and Interchromophore excitation transfer. *J. Phys. Chem.* **1994**, *98*, 4580–4590.
- (52) Rist, M.; Wagenknecht, H.-A.; Fiebig, T. Exciton and excimer formation in DNA at room temperature. *ChemPhysChem* **2002**, *3*, 704–707.
- (53) Slifkin, M. A. *Charge Transfer Interactions of Biomolecules*; Academic Press: London, 1971.
- (54) Levine, B. G.; Martinez Todd, J. Isomerization through conical intersections. *Annu. Rev. Phys. Chem.* **2007**, *58*, 613–634.
- (55) Yarkony, D. R. Conical Intersections: The New Conventional Wisdom. *J. Phys. Chem. A* **2001**, *105*, 6277–6293.
- (56) Matsika, S. Conical intersections in molecular systems. *Rev. Comput. Chem.* **2007**, *23*, 83–124.
- (57) Domcke, W.; Yarkony, D. R.; Koppel, H. *Conical Intersections: Electronic Structure, Dynamics, and Spectroscopy*; World Scientific Publishing Co.: Hackensack, NJ, 2004.
- (58) Robb, M. A.; Garavelli, M.; Olivucci, M.; Bernardi, F. *A Computational Strategy for Organic Photochemistry*; Wiley-VCH: New York, 2000; Vol. 15.
- (59) Pullman, B. In *Molecular Associations in Biology*; Pullman, B., Ed.; Academic Press: New York, 1967.
- (60) Parsons, W. W. *Modern Optical Spectroscopy*; Springer: Berlin, Heidelberg, 2007.
- (61) Sutin, N. Theory of electron transfer reactions: insights and hindsights. *Prog. Inorg. Chem.* **1983**, *30*, 441–498.

JP1011507